COMPDYN 2013
4th ECCOMAS Thematic Conference on
Computational Methods in Structural Dynamics and Earthquake Engineering
M. Papadrakakis, V. Papadopoulos, V. Plevris (eds.)
Kos Island, Greece, 12–14 June 2013

AN IMPROVED METHODOLOGY FOR THE VIRTUAL POINT TRANSFORMATION OF MEASURED FREQUENCY RESPONSE FUNCTIONS IN DYNAMIC SUBSTRUCTURING

Maarten V. van der Seijs[1], Daniël D. van den Bosch[1], Daniel J. Rixen[2] and Dennis de Klerk[1]

[1]Delft University of Technology
Faculty of Mechanical, Maritime and Materials Engineering, Section of Engineering Dynamics
Mekelweg 2, 2628CD, Delft, The Netherlands
e-mail: m.v.vanderseijs@tudelft.nl

[2]Technische Universität München
Faculty of Mechanical Engineering, Institute of Applied Mechanics
Boltzmannstr. 15, D - 85748 Garching, Germany
e-mail: rixen@tum.de

Keywords: Frequency Based Substructuring, Experimental Substructuring, NVH, Virtual Point Transformation

Abstract. *Dynamic Substructuring methods play a significant role in the analysis of todays complex systems. Crucial in Dynamic Substructuring is the correct definition of the interfaces of the subsystems and the connectivity between them. Although this is straightforward practice for numerical finite element models, the experimental equivalent remains challenging. One of the issues is the coupling of the rotations at the interface points that cannot be measured directly. This work presents a further extension of the virtual point transformation that is based on the Equivalent Multi-Point Connection (EMPC) method and Interface Deformation Mode (IDM) filtering. The Dynamics Substructuring equations are derived for the weakened interface problem. Different ways to minimise the residuals caused by the IDM filtering will be introduced, resulting in a controllable weighting of measured Frequency Response Functions (FRFs). Also some practical issues are discussed related to the measurement preparation and post-processing. Special attention is given to sensor and impact positioning. New coherence-like indicators are introduced to quantify the consistency of the transformation procedures: sensor consistency, impact consistency and reciprocity.*

1 INTRODUCTION

Dynamic Substructuring (DS) has proven to be a powerful engineering tool for a wide variety of industries. It allows a complex dynamic system to be modelled and analysed as separate components or "substructures", building a bridge between the efforts of different suppliers and design groups. Also, components may be coupled from either numerical or experimental nature. The first class is often characterised by finite element models or reduced-order models, that tend to be relatively easy to assemble and highly controllable in terms of numerical accuracy. Substructuring methods associated with these models are numerous and have been well accepted over the last decades [2]. However, with increasing product complexity, the question rises how truthful some numerical models represent the actual behaviour of the components. Experimental identification of components is therefore often desired for the purpose of model validation.

In recent years though, an increasing amount of research has been devoted to substructuring with the experimental models themselves, leading to hybrid and very powerful modelling methodologies [4, 11]. Although the substructuring techniques themselves are formulated in a rather straightforward way (see for instance [5]), the largest challenges exist in the coupling of the measured components. To couple substructures properly, one requires a complete and accurate model of the dynamics at the interface for both translational and rotational degrees of freedom [8, 12, 13].

1.1 Modelling the interface problem

The DS algorithm requires that displacement compatibility and force equilibrium is explicitly satisfied on the interfaces of the connected substructures. In a discretised world, coupling could be fully determined by imposing this two conditions on the respective coupling nodes of the substructures.

However in industrial practice components are often connected by bolts or welds, that physically show more resemblance to a line or surface connection than to a single point. Modelling a continuous contact surface or line is of course not feasible as one would theoretically need an infinite amount of DoFs. It is therefore common practice to reduce the interface problem to one or more connecting nodes.

Let us for example consider a substructure connection as illustrated in figure 1a. If both structures would be represented by an FE model, the substructuring task amounts to coupling the displacements and interface forces of the coinciding nodes (figure 1b). By coupling a sufficient number of nodes over a larger area, any rotational coupling is implicitly accounted for.

However in connecting experimental substructures very few guidelines exist. A simple triaxial translational Single-Point Connection (SPC) is simply inadequate to couple the rotational degrees of freedom (RDoFs). To overcome the RDoF problem, it was suggested by [6] and [14] to introduce an Equivalent Multi-Point Connection (EMPC) as illustrated by figure 1c. This method couples the translational directions of multiple points in the proximity of the interface which implicitly accounts for the rotations. In practice, a minimum of 3 triaxial accelerometers (not in line) is sufficient to fully determine the 6 DoF coupling, i.e. 3 translational and 3 rotational directions.

1.2 Weakening the interface conditions

Unfortunately it was observed that the 9 DoFs resulting from a 3-point coupling may even overdetermine the coupling problem. As the structure between the 3 connections point is typ-

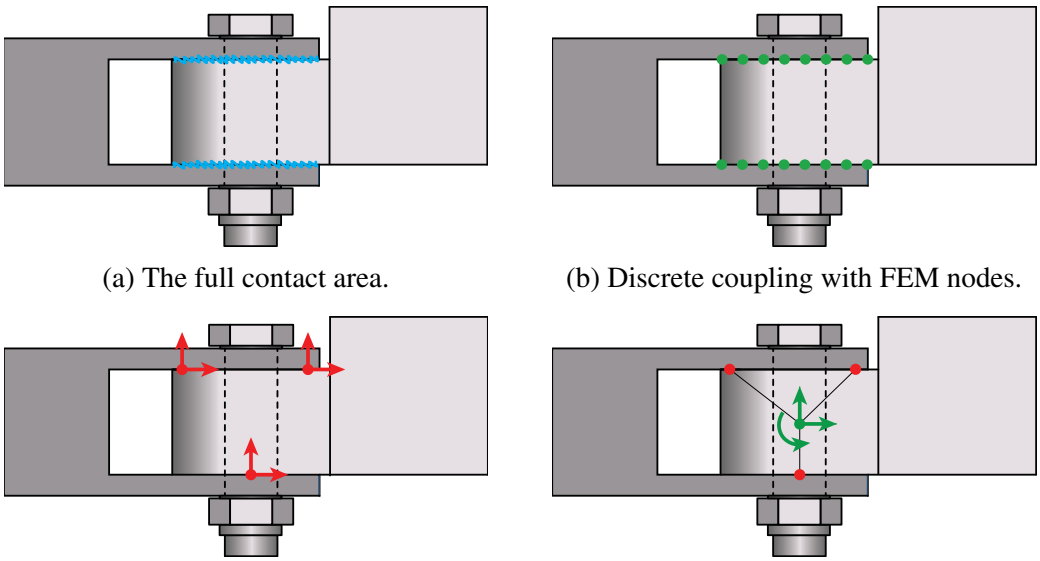

(a) The full contact area.

(b) Discrete coupling with FEM nodes.

(c) Standard EMPC: multiple points, only translational directions (9 DoFs).

(d) Extended EMPC: One virtual point, 3 translations and 3 rotations (9 $\rightarrow$ 6 DoFs).

Figure 1: A bolted connection: three ways to model the interface problem.

ically very stiff, any discrepancy in motion (often due to measurement errors) will be over-compensated for in the DS coupling equations, resulting in unwanted "stiffening" and spurious peaks in the coupled FRFs [15].

In fact the local rigidness of the interface is the essential observation that leads to the concept of Interface Deformation Mode (IDM) filtering, as introduced in the same work. By defining 6 rigid IDMs per interface and projecting the 9-DoF (or more) receptance matrix onto this subspace, one only retains the dynamics that load the interface area in a rigid manner. When substructuring is performed with this "filtered" receptance, one only imposes the compatibility and equilibrium conditions on the motion of those 9 DoFs that obey local rigid behaviour, while the residual flexible motion is left uncoupled. In effect the interface problem is "weakened" and, due to the least-square reduction step, measurement errors are averaged out.

1.3 Virtual point description

More generally, one can look at this concept from a modal reduction point of view and simply describe the rigid interface dynamics using the generalised set of coordinates associated with the rigid IDMs. Doing so, one has in fact obtained a 6-DoF per node receptance model that is directly compatible for coupling with FE models. This is illustrated by figure 1d. Indeed, the nodal 6×6 receptance matrices describe the dynamic responses between the so-called *virtual point displacements* and *virtual point forces*: the receptance of the interface concentrated in a virtual point[1].

Interesting is now how to set up an experiment that leads to a complete and reciprocal 6×6 virtual point FRF matrix, including proper "driving-point" receptance on the diagonal. Various studies have dealt with problems related to driving-point measurements [10, 16] and the propagation of measurement errors into the coupled FRFs [7, 15].

[1]The point is said to be virtual, since no actual measurements have been done on this point and it can in fact be chosen anywhere in the proximity of the interface.

1.4 Paper outline

This paper discusses the virtual point transformation that translates the measured (impact) forces and displacements to virtual point receptance. The theoretical background on dynamic substructuring and the virtual point transformation is provided in section 2. Next, section 3 aims at providing some practical guidelines to set up an experiment and means to evaluate the results of the measurements in terms of consistency of the transformation and resulting reciprocity. The paper is concluded with a short summary in section 4.

2 THEORY

The Virtual Point Transformation is based on the theory of the Equivalent Multi-Point Connection (EMPC) method. This method was first presented by [6, 14, 17]. A physical derivation of the transformation and ways to construct IDM matrices for individual subsystems were suggested by [16]. In this work however, the virtual point transformation is approached slightly differently, namely from a Dynamic Substructuring point of view. Thereafter the physical derivation of the IDM matrices is discussed.

2.1 Dynamic Substructuring with weakened interface conditions

Dynamic substructuring connects substructures by imposing two conditions: compatibility of interface displacements and equilibrium of interface forces. For the derivation of the virtual point transformation, let us first consider a simple coupling problem of two substructures A and B, characterised by their FRF matrices $\mathbf{Y}^{\mathrm{A}}(\omega)$ and $\mathbf{Y}^{\mathrm{B}}(\omega)$. In summary, one can start with writing the dynamic equations of the uncoupled system using a block-diagonal receptance matrix $\mathbf{Y} = \mathrm{diag}(\mathbf{Y}^{\mathrm{A}}, \mathbf{Y}^{\mathrm{B}})$, such that the uncoupled responses $\mathbf{u} = [\mathbf{u}^{\mathrm{A}}; \mathbf{u}^{\mathrm{B}}]$ to some force loading $\mathbf{f}^{tot}$ are found by[2]:

$$\mathbf{u} = \mathbf{Y}\mathbf{f}^{tot} \tag{1}$$

The total forces $\mathbf{f}^{tot}$ are typically a combination of external loads $\mathbf{f}$ and interface forces $\mathbf{g}$. Let us for now imagine that the interface nodes of the two substructures coincide perfectly, such that the compatibility condition can be stated by equating the translational DoFs of the two substructure boundaries $\mathbf{u}_b^{\mathrm{A}} = \mathbf{u}_b^{\mathrm{B}}$ or $\mathbf{B}\mathbf{u} = \mathbf{0}$, using the signed boolean matrix notation (see [5]). The following coupled system of equations is then obtained:

$$\mathbf{u} = \mathbf{Y}(\mathbf{f} + \mathbf{g}) = \mathbf{Y}(\mathbf{f} - \mathbf{B}^T\boldsymbol{\lambda}) \tag{2a}$$

$$\mathbf{B}\mathbf{u} = \mathbf{0} \tag{2b}$$

where the interface forces are expressed using the same matrix $\mathbf{B}$ and a set of Lagrange multipliers $\boldsymbol{\lambda}$ that are yet unknown.

2.1.1 Interface reduction

Let us now imagine that one is interested in considering the interface displacements as rigid, or at least represented by some more general Interface Deformation Modes (IDMs) contained in the $N \times M$ matrix $\mathbf{R}$ with modal coordinates $\mathbf{q}$. As the number of IDMs is smaller than the number of interface DoFs ($M < N$), a residual on the displacements $\boldsymbol{\mu}$ is added:

$$\mathbf{u} = \mathbf{R}\mathbf{q} + \boldsymbol{\mu} \tag{3}$$

[2] In this derivation the explicit frequency dependency of $\mathbf{Y}(\omega)$, $\mathbf{u}(\omega)$ and $\mathbf{f}(\omega)$ is omitted for clarity.

To find $\mathbf{q}$ in a minimal sense, one could directly apply the (Moore-Penrose) pseudo-inverse of $\mathbf{R}$, minimising the norm of the residuals on the displacements. Instead one can also introduce a symmetric weighting matrix $\mathbf{W}$ that can be chosen to have the residual satisfying

$$\mathbf{R}^T\mathbf{W}\boldsymbol{\mu} = \mathbf{0} \tag{4}$$

such that the coordinate transformation and filtering process becomes:

$$\mathbf{R}^T\mathbf{W}\mathbf{u} = \mathbf{R}^T\mathbf{W}\mathbf{R}\mathbf{q} \tag{5a}$$

$$\mathbf{q} = \left(\mathbf{R}^T\mathbf{W}\mathbf{R}\right)^{-1}\mathbf{R}^T\mathbf{W}\mathbf{u} \tag{5b}$$

$$\tilde{\mathbf{u}} = \mathbf{R}\left(\mathbf{R}^T\mathbf{W}\mathbf{R}\right)^{-1}\mathbf{R}^T\mathbf{W}\mathbf{u} \tag{5c}$$

or short:

$$\mathbf{q} = \mathbf{T}\mathbf{u} \qquad \text{with} \qquad \mathbf{T} \triangleq \left(\mathbf{R}^T\mathbf{W}\mathbf{R}\right)^{-1}\mathbf{R}^T\mathbf{W} \tag{6a}$$

$$\tilde{\mathbf{u}} = \mathbf{R}\mathbf{T}\mathbf{u} = \mathbf{P}\mathbf{u} \qquad \text{with} \qquad \mathbf{P} \triangleq \mathbf{R}\left(\mathbf{R}^T\mathbf{W}\mathbf{R}\right)^{-1}\mathbf{R}^T\mathbf{W} \tag{6b}$$

Vector $\tilde{\mathbf{u}}$ denotes the physical displacements projected onto the IDM subspace. $\mathbf{P}$ is the $N \times N$ projection operator of reduced rank $M < N$.

Note that the above procedure is in fact a least-square projection minimising the squared error $\boldsymbol{\mu}^T\mathbf{W}\boldsymbol{\mu}$. If $\mathbf{W}$ is chosen to be identity, the pseudo-inverse is found, $\mathbf{T} = (\mathbf{R}^T\mathbf{R})^{-1}\mathbf{R}^T$, which leads to a minimisation of the error on the displacements. In general if $\mathbf{W}$ is a diagonal matrix, it gives weight to the individual displacements in the error minimisation such that one can control the importance of a certain DoF for the transformation. However if $\mathbf{W}$ is chosen to represent a (dynamic) stiffness matrix, one is nullifying some local residual energy. Alternative choices for $\mathbf{W}$ are beyond the scope of this paper.

2.1.2 Substructure assembly

The interface reduction as derived above allows us to assemble only the rigid behaviour of the interface ($\tilde{\mathbf{u}} = \mathbf{R}\mathbf{q}$) that was properly measured. The rest ($\boldsymbol{\mu}$) is left free, being either measurement noise or higher-order deformations that one could probably not measure correctly due to inaccuracies in impact and sensor locations.

Rewriting the dual DS equations of (2a) and (2b) for rigid interface coupling:

$$\mathbf{u} = \mathbf{Y}(\mathbf{f} + \mathbf{g}) \tag{7a}$$

$$\mathbf{B}\mathbf{q} = \mathbf{B}\left(\mathbf{R}^T\mathbf{W}\mathbf{R}\right)^{-1}\mathbf{R}^T\mathbf{W}\mathbf{u} = \mathbf{0} \tag{7b}$$

The boolean matrix $\mathbf{B}$ is different to the one of (2b) as it now couples the DoFs of the rigid IDMs, hence the rigid behaviour of $\mathbf{u}$. The forces $\mathbf{g}$ are still coupling forces in the unreduced domain but conjugate to the IDM conditions, namely:

$$\mathbf{g} = -\mathbf{W}^T\mathbf{R}\left(\mathbf{R}^T\mathbf{W}\mathbf{R}\right)^{-1}\mathbf{B}^T\boldsymbol{\lambda} = -\mathbf{T}^T\mathbf{B}^T\boldsymbol{\lambda} \tag{8}$$

and the coupled system becomes:

$$\mathbf{u} = \mathbf{Y}(\mathbf{f} - \mathbf{T}^T\mathbf{B}^T\boldsymbol{\lambda}) \tag{9a}$$

$$\mathbf{B}\mathbf{q} = \mathbf{B}\mathbf{T}\mathbf{u} = \mathbf{0} \tag{9b}$$

Writing now the first equation in the second and solving for $\boldsymbol{\lambda}$:

$$\mathbf{BTYf} - \mathbf{BTYT}^T\mathbf{B}^T\boldsymbol{\lambda} = \mathbf{0}$$

$$\boldsymbol{\lambda} = \left(\mathbf{BTYT}^T\mathbf{B}^T\right)^{-1}\mathbf{BTYf} \tag{10}$$

Putting everything together in (9a) gives us the dynamic equation for the reduced-interface coupling:

$$\mathbf{u} = \mathbf{Yf} - \mathbf{YT}^T\mathbf{B}^T\left(\mathbf{BTYT}^T\mathbf{B}^T\right)^{-1}\mathbf{BTYf} \tag{11}$$

The receptance matrix of the coupled system is given by

$$\mathbf{Y}^{ass} = \mathbf{Y} - \mathbf{YT}^T\mathbf{B}^T\left(\mathbf{BTYT}^T\mathbf{B}^T\right)^{-1}\mathbf{BTY} \tag{12}$$

such that we can simplify to $\mathbf{u} = \mathbf{Y}^{ass}\mathbf{f}$.

2.2 Dynamic Substructuring with virtual point DoFs

Equation (11) gives the coupled reduced-interface dynamic equations for the physical displacements and forces $\mathbf{u}$ and $\mathbf{f}$. However when coupling the experimental models to FE models or even to each other, it is probably more convenient to set up the substructuring equations using the virtual point DoFs directly. Let us therefore state the relation between measured and virtual displacements and forces once more:

$$\mathbf{q} = \left(\mathbf{R}^T\mathbf{WR}\right)^{-1}\mathbf{R}^T\mathbf{Wu} = \mathbf{Tu} \tag{13a}$$

$$\mathbf{f} = \mathbf{W}^T\mathbf{R}\left(\mathbf{R}^T\mathbf{WR}\right)^{-1}\mathbf{m} = \mathbf{T}^T\mathbf{m} \tag{13b}$$

The first equation was already defined by (5b). The second equation to obtain the virtual forces $\mathbf{f}$ uses the same $\mathbf{T}$ as the virtual displacements and therefore the same IDMs[3]. However a different $\mathbf{T}$ could easily be constructed, as long as the IDM coordinates match: the components in $\mathbf{m}$ are indeed a force or torque in the direction of the components of $\mathbf{q}$. More detail on how to obtain the IDMs for the sensors and impacts is found in section 2.3.

Combining equations (11), (13a) and (13b) gives us the coupled system equations in terms of the virtual point displacements $\mathbf{q}$ and forces $\mathbf{m}$:

$$\mathbf{q} = \mathbf{TYT}^T\mathbf{m} - \mathbf{TYT}^T\mathbf{B}^T\left(\mathbf{BTYT}^T\mathbf{B}^T\right)^{-1}\mathbf{BTYT}^T\mathbf{m} \tag{14}$$

Observes that compared to equation (11) the applied forces are now also filtered, so that only the resulting virtual forces corresponding to the IDM subspace are implied in the dynamic computations.

Substituting $\mathbf{H} = \mathbf{TYT}^T$ as a virtual point receptance matrix, we get:

$$\mathbf{q} = \mathbf{Hm} - \mathbf{HB}^T\left(\mathbf{BHB}^T\right)^{-1}\mathbf{BHm} \tag{15}$$

and as a result

$$\mathbf{H}^{ass} = \mathbf{H} - \mathbf{HB}^T\left(\mathbf{BHB}^T\right)^{-1}\mathbf{BH} \tag{16}$$

which has exactly the same form as the well-known Lagrange Multiplier FBS formula [5] but now for the virtual point dynamics. Indeed $\mathbf{H}(\omega)$ comprises the virtual point receptance relating the virtual point forces $\mathbf{m}(\omega)$ to virtual point displacements $\mathbf{q}(\omega)$. Due to the block-diagonal construction of the subsystem IDM matrices, we can also conclude that $\mathbf{H} = \mathrm{diag}(\mathbf{H}^{\mathrm{A}}, \mathbf{H}^{\mathrm{B}})$, showing that the virtual point receptance can be built up for the subsystems independently.

[3]This implies that the locations of the applied forces (hammer impacts or shaker excitations) should completely coincide with the corresponding measured responses (sensors).

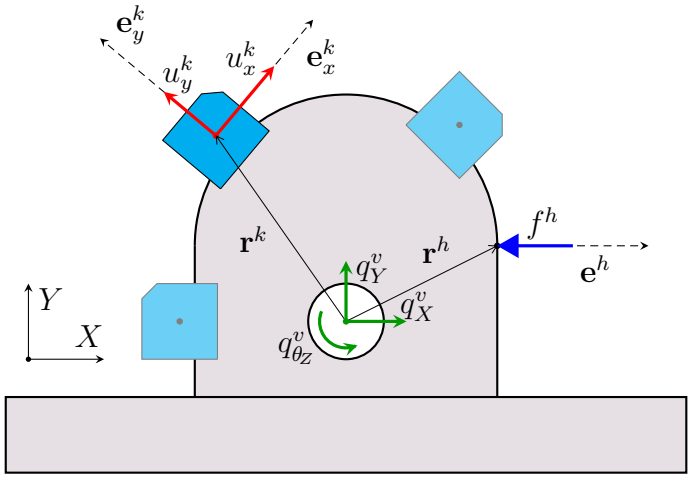

Figure 2: The IDMs associated with the virtual point (green) can be constructed from the positions and directions of the measured displacements (red) and impacts (blue).

2.3 Construction of the Interface Displacement Modes

In the derivation above it was shown that the virtual point transformation relies on a reduction in a modal sense, namely reducing the interface connectivity using a set of Interface Deformation Modes (IDMs) specified by $\mathbf{R}$. Let us now elaborate on how to obtain these IDMs for a single interface indicated in figure 2. Virtual point v is surrounded by $N_k = 3$ triaxial acceleration sensors, registering a total of 9 translational displacements[4] in the local (x, y, z) frame of the sensors. An impact is indicated by a thick blue arrow.

2.3.1 Displacements

Following equation (3) the sensor IDM matrix $\mathbf{R}$ translates the local frame displacements to 6 virtual point displacements and rotations plus a residual. Let us write out this equation for a triaxial sensor k. The orientation of the sensor is determined by its three measurement directions specified as the unit vectors $[\ \mathbf{e}_x^k\ \ \mathbf{e}_y^k\ \ \mathbf{e}_z^k\ ] = \mathbf{E}^k$ while the distance from the sensor to the virtual point is given by vector $\mathbf{r}^k$. The respective local displacements along these directions are denoted by $\mathbf{u}^k$. The 6 DoFs of virtual point v are contained in the set $\mathbf{q}^v$.

$$\begin{bmatrix} u_x^k \\ u_y^k \\ u_z^k \end{bmatrix} = \begin{bmatrix} e_{x,X}^k & e_{x,Y}^k & e_{x,Z}^k \\ e_{y,X}^k & e_{y,Y}^k & e_{y,Z}^k \\ e_{z,X}^k & e_{z,Y}^k & e_{z,Z}^k \end{bmatrix} \begin{bmatrix} 1 & 0 & 0 & 0 & r_Z^k & -r_Y^k \\ 0 & 1 & 0 & -r_Z^k & 0 & r_X^k \\ 0 & 0 & 1 & r_Y^k & -r_X^k & 0 \end{bmatrix} \begin{bmatrix} q_X^v \\ q_Y^v \\ q_Z^v \\ q_{\theta_X}^v \\ q_{\theta_Y}^v \\ q_{\theta_Z}^v \end{bmatrix} + \begin{bmatrix} \mu_x^k \\ \mu_y^k \\ \mu_z^k \end{bmatrix} \tag{17}$$

Introducing $\bar{\mathbf{R}}^{kv}$ as the 3×6 global frame matrix associated with sensor k and virtual point v, we can write:

$$\mathbf{u}^k = \mathbf{E}^{k^T} \bar{\mathbf{R}}^{kv} \mathbf{q}^v + \boldsymbol{\mu}^k \tag{18}$$

$$\mathbf{u}^k = \mathbf{R}^{kv} \mathbf{q}^v + \boldsymbol{\mu}^k \qquad \text{with} \qquad \mathbf{R}^{kv} = \mathbf{E}^{k^T} \bar{\mathbf{R}}^{kv} \tag{19}$$

[4] In fact the sensors measure accelerations but for simplicity of notation displacements are considered here.

For a typical problem having 3 sensors per virtual point and sorted in ascending virtual point order, the $\mathbf{R}^{kv}$ matrices can be stacked to form the following equations[5]:

$$\mathbf{u} = \mathbf{R}\mathbf{q} + \boldsymbol{\mu} \qquad \text{with} \qquad \mathbf{R} = \begin{bmatrix} \mathbf{R}^{1,1} & & & \\ \mathbf{R}^{2,1} & & & \\ \mathbf{R}^{3,1} & & & \\ & \mathbf{R}^{4,2} & & \\ & \mathbf{R}^{5,2} & & \\ & \mathbf{R}^{6,2} & & \\ & & \ddots & \\ & & & \mathbf{R}^{N_k,N_v} \end{bmatrix} \tag{20}$$

Alternatively one may prefer to describe the virtual point relation per measurement direction individually, such that a single displacement DoF u_i^k in the local direction $\mathbf{e}_i^k$ can be related to the associated set of virtual point coordinates in $\mathbf{q}^v$:

$$u_i^k = \begin{bmatrix} \mathbf{e}_i^{kT} & \left(\mathbf{r}_i^k \times \mathbf{e}_i^k\right)^T \end{bmatrix} \mathbf{q}^v + \mu_i^k = \mathbf{R}_i^{kv}\mathbf{q}^v + \mu_i^k \tag{21}$$

from which the full matrix $\mathbf{R}$ can be assembled row-wise per sensor channel i and column-wise for the different virtual points.

Regardless of the construction method the resulting IDM matrix $\mathbf{R}$ shall be block diagonal, or at least have IDMs that are uncoupled over the various virtual points and sensor groups (if a different ordering was used). Although not treated here, $\mathbf{R}$ may be augmented with flexible IDMs if desired. Note that in any case one should take care that $\mathbf{R}$ is at least full rank (but preferably overdetermined) such that a (generalised) inverse $\mathbf{T}$ can be computed by applying equation (13a):

$$\mathbf{q} = \left(\mathbf{R}^T\mathbf{W}\mathbf{R}\right)^{-1}\mathbf{R}^T\mathbf{W}\mathbf{u} = \mathbf{T}\mathbf{u}$$

2.3.2 Forces

The transformation of the forces can be performed in a similar step-wise way. Unlike displacements, forces are not uniquely defined by virtual point forces and moments (from here on simply called virtual forces). In fact the other way around is true, such that the following relation can be written for the set of virtual forces $\mathbf{m}^v$ as a result of an impact f^h in the direction of $\mathbf{e}^h$ at distance $\mathbf{r}^h$:

$$\begin{bmatrix} m_X^v \\ m_Y^v \\ m_Z^v \\ m_{\theta_X}^v \\ m_{\theta_Y}^v \\ m_{\theta_Z}^v \end{bmatrix} = \begin{bmatrix} 1 & 0 & 0 \\ 0 & 1 & 0 \\ 0 & 0 & 1 \\ 0 & -r_Z^h & r_Y^h \\ r_Z^h & 0 & -r_X^h \\ -r_Y^h & r_X^h & 0 \end{bmatrix} \begin{bmatrix} e_X^h \\ e_Y^h \\ e_Z^h \end{bmatrix} f^h \tag{22}$$

Now we like to use similar notation as (21), but to do so we need the transpose of $\mathbf{R}^{hv}$:

$$\mathbf{m}^v = \begin{bmatrix} \mathbf{e}^h \\ \mathbf{r}^h \times \mathbf{e}^h \end{bmatrix} f^h = \mathbf{R}^{hv^T} f^h \tag{23}$$

[5] it is easy to observe that if only translational information is desired for a certain virtual point (e.g. if one only used one sensor), the sensor rotation matrix can be used directly: $\mathbf{R}^{kv} = \mathbf{E}^{k^T}$.

Every impact adds a single column to the IDM matrix $\mathbf{R}^T$. Assuming 9 impacts per virtual point, the system for the complete set of DoFs is constructed as follows:

$$\mathbf{m} = \mathbf{R}^T\mathbf{f} \qquad \text{with} \qquad \mathbf{R} = \begin{bmatrix} \mathbf{R}^{1,1} & & & \\ \vdots & & & \\ \mathbf{R}^{9,1} & & & \\ & \mathbf{R}^{10,2} & & \\ & \vdots & & \\ & \mathbf{R}^{18,2} & & \\ & & \ddots & \\ & & & \mathbf{R}^{N_h,N_v} \end{bmatrix} \tag{24}$$

Note that the transpose of the IDM matrix of the forces takes the same form as the IDM matrix of the displacements from equation (20). In fact if one decides to excite only on the sensor faces (which is generally not advised, see section 3.2), one has the exact same IDM matrix apart from some sign changes.

With more than independent 6 excitations per virtual point, equation (24) becomes underdetermined, which means that there is no unique combination of the impacts $\mathbf{f}$ from which a certain $\mathbf{m}$ can be constructed. Again the solution is found by using a generalised inverse, only this time a weighted "right inverse":

$$\mathbf{f} = \mathbf{W}^T\mathbf{R}\left(\mathbf{R}^T\mathbf{W}\mathbf{R}\right)^{-1}\mathbf{m} = \mathbf{T}^T\mathbf{m} \tag{25}$$

that can be shown to minimise the error on the residual impact forces weighted by $\mathbf{W}$. We can now see that the underdetermination of (24) in fact reflects an overdetermination of the inversed problem of (25), which again has advantageous properties for interface weakening and error suppression as discussed in section 2.1.

3 PRACTICE

This section will elaborate on some more practical issues related to virtual point modelling. Proper positioning of the sensors and impacts has to be taken into consideration. Much care should be taken to ensure that all 6 DoFs per virtual point can be described independently. This has implications for both sensor placement and impact positions. After measuring some careful post-processing needs to be done to come up with good results. The following preparation and post-processing steps are presented in the order as they may normally appear in time.

3.1 Sensor placement

The thought that two triaxial sensors (measuring two times 3 translations) can completely describe the 6 DoF virtual point, can be deceiving. When the responses of two triaxial sensors are transformed to a 6 DoF virtual point description, one linear dependence will always appear in the virtual points DoFs. This linear dependence is caused by the fact that the triaxial sensors are unable to describe the rotation over the axis spanned between both sensors as illustrated by figure 3a. This is regardless of the position of the sensors relative to the virtual point. Adding a third triaxial sensor, such that the three sensors span a surface (figure 3b), enables the three sensors with a total of 9 DoFs to describe all 6 DoFs of the virtual point.

The additional benefit of the third triaxial sensor is of course the overdetermination of the interface problem. Using the virtual point transformation as discussed in section 2 the effects of

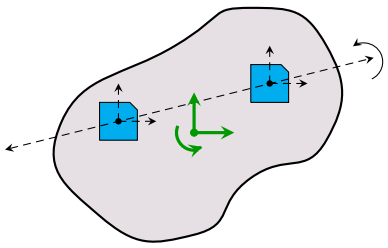

(a) Two sensors spanning a line: one dependency between the rotational axes.

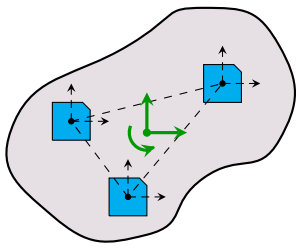

(b) Three sensors spanning a surface: all rotations fully determined.

uncorrelated measurement noise as well as errors due to misalignment of the sensor are reduced, which is generally considered a good practice [6, 9, 16]. The use of at least three triaxial sensors per virtual point can therefore be held as rule of thumb.

Finally, considering the rigid interface assumption, it seems evident that it would be best practice to place the sensors as close as possible to the virtual point. The smaller the distances are, the smaller the effects of flexible interface modes are compared to the rigid interface motion. On the other hand, for smaller distances, the virtual point transformation will get more sensitive to to absolute errors on the position. In general one should approach this matter with some engineering judgement or foreknowledge about the system.

3.2 Impact positions

Unlike the 6 displacements measured by 2 triaxial sensors, 6 well-positioned force impacts could in practice be sufficient to fully determine the 6 generalised forces at the virtual point. Still, for the same reason, it is wise to choose more excitation points that overdetermine the force transformation.

Similar to the sensor placement, three impacts in each direction (X, Y, Z) can be used as a rule of thumb. Also one should include excitations of which the direction normal ($\mathbf{e}^h$) does not point straight to the virtual point, in order to create "moment" along the rotational axes.

In some previous studies the sensor faces were chosen as possible impact locations [3, 16]. Depending on the chosen sensors this can have its advantages and disadvantages. Since the impact locations and directions are equal to the locations and orientations of the measured XYZ responses in the sensor, the same transformation matrix can be used for both transformations. However, practice shows that FRFs obtained at the driving point exhibit poor coherence, especially for the cross-directional FRFs of one sensor. Also, the sensor is easily driven in overload. As the virtual point transformation does not require physical driving-point receptance, this type of excitations should be avoided.

It seems logical to apply the impacts as close as possible to the virtual point in order to avoid inducing local deformation around the virtual point, but an the other hand one wants to be far enough to be less sensitive to errors in the impact location and orientation. The same reasoning as for the sensor placement holds here.

3.3 Post-processing

After measuring, the obtained FRF data should be organised into a matrix $\mathbf{Y}(\omega)$ such that the virtual point transformation can be performed:

$$\mathbf{H}(\omega) = \mathbf{T}\mathbf{Y}(\omega)\mathbf{T}^T$$

The transformation matrices $\mathbf{T}$ left and right from the receptance matrix denote respectively the sensor and impact transformation matrices as constructed from the IDMs[6]. In practice these steps involve accurate determination of the positions and orientations (directions) of both the sensors and impacts. Besides ruler and calliper measurement, optical measurement systems as well as CAD models of the components at hand may dramatically improve the accuracy of the position determination and with that the quality of the transformation. The use of such assisting systems is therefore strongly suggested.

3.4 Performance indicators

In section 2 the relation between measured and virtual displacements and forces was set up. The residuals that result from the least-square projection of the measured receptance data can be used to derive a meaningful value to evaluate the accuracy of the sensor and impacts positions.

3.4.1 Sensor consistency

In order to say something about the how the consistency of the sensor placement and the constructed IDMs, let us get back to the the interface reduction equation of (3):

$$\mathbf{u} = \mathbf{R}\mathbf{q} + \boldsymbol{\mu}$$

We define $\mathbf{f}_h$ as the "load case" resulting from a unit impact somewhere at the structure, reasonably far away from virtual point 1. Then the measured responses of the sensors associated with virtual point 1 due to the given load case are:

$$\mathbf{u}_1(\mathbf{f}_h) = \mathbf{Y}_1\mathbf{f}_h = \mathbf{Y}_{1h}$$

which is simply the receptance column corresponding to that impact. For substructure coupling, we are interested in the filtered responses $\tilde{\mathbf{u}}_1$ due to the transformation via $\mathbf{q}_1$:

$$\tilde{\mathbf{u}}_1(\mathbf{f}_h) = \mathbf{R}_{11}\mathbf{q}_1(\mathbf{f}_h) = \mathbf{R}_{11}\mathbf{T}_{11}\mathbf{u}_1(\mathbf{f}_h) = \mathbf{P}_{11}\mathbf{Y}_{1h}$$

Now, we are able to compare $\mathbf{u}_1$ with $\tilde{\mathbf{u}}_1$ using a formulation similar to the Modal Assurance Criterion [1]:

$$\rho^2_{\mathbf{u}_1} = \mathrm{MAC}\left(\tilde{\mathbf{u}}_1(\mathbf{f}_h), \mathbf{u}_1(\mathbf{f}_h)\right) = \mathrm{MAC}\left(\mathbf{P}_{11}\mathbf{Y}_{1h}, \mathbf{Y}_{1h}\right) \tag{26}$$

with

$$\mathrm{MAC}(\mathbf{a}, \mathbf{b}) \triangleq \frac{(\mathbf{a}^H\mathbf{b})(\mathbf{b}^H\mathbf{a})}{(\mathbf{a}^H\mathbf{a})(\mathbf{b}^H\mathbf{b})} \tag{27}$$

The value $\rho^2_{\mathbf{u}_1}$ is called the *sensor consistency* (in previous work *rigidness* [6, 16]) and gives a value between 0 and 1 that indicates how well the sensors of virtual point 1 can describe the dynamics (caused by a certain excitation) through the IDM modes. It is a frequency dependent indicator that can be evaluated for every virtual point and for each excitation separately[7]. Evaluating the sensor coherence for several impacts provides meaningful insights in the consequences of the transformation. Low sensor consistency can have the following causes:

[6] In general the two $\mathbf{T}$ matrices are different and depend on the sensor and impact locations, see section 2.3.

[7] An excitation $\mathbf{f}_2$ "far away" from the virtual point of interest is suggested because then one observes the global response to some force that brought the complete system in motion, rather then a response that may be highly affected by impact position differences in the vicinity of the virtual point of interest.

- The position and orientation of a sensor was not properly determined, such that the measured kinematics appear incompatible with the IDM kinematics. If for instance one sensor is rotated 90 degrees along the Z-axis, a rigid interface motion in the X, Y-plane will appear as a partly flexible motion. The effect will be visible as a low consistency over the full frequency range.
- The interface area spanned between the sensors is flexible, such that the rigid IDMs cannot fully describe the dynamics. This will mostly reflect in reduced consistency for increasing frequencies.
- If the rigidness is particularly low for a certain impact, one may question if this impact was either to soft (low signal-to-noise-ratio) or to strong (driving on or more sensors in overload). In such cases it is preferred to leave this impact (column of $\mathbf{Y}$) out of the transformation.

Note that the sensor consistency requires an overdetermination of the problem, otherwise it will just indicate a straight value of 1.

3.4.2 Impact consistency

Similar to the sensor consistency, it is possible to come up with a consistency measure for the applied forces. This value is especially valuable to assess the accuracy of the impact positions and by that the consistency of the force IDMs.

This time we are interested in the responses of a single sensor channel u_i to all the impacts of virtual point 1, which is equal to a row of the measured receptance matrix:

$$u_i(\mathbf{f}_1) = \big(u_i(f_1), u_i(f_2), \ldots, u_i(f_9)\big) = \mathbf{Y}_{i1}$$

The response to the filtered set of impacts, i.e. the combination of impacts that only result in a rigid load, is found by applying the projection matrix for the force IDMs:

$$u_i(\tilde{\mathbf{f}}_1) = \mathbf{Y}_{i1}\mathbf{P}_{11}$$

The *impact consistency* is then defined by:

$$\rho^2_{\mathbf{f}_1} = \mathrm{MAC}\left(u_i(\tilde{\mathbf{f}}_1), u_i(\mathbf{f}_1)\right) = \mathrm{MAC}\left(\mathbf{Y}_{i1}\mathbf{P}_{11}, \mathbf{Y}_{i1}\right) \tag{28}$$

Also, this value is limited between 0 and 1.

3.4.3 Reciprocity

Evaluating sensor and hammer impact consistency can be useful to find errors in the measurement setup, calibration, etc. However a high consistency does not guarantee reciprocity of virtual point FRFs. Reciprocity of the raw measurement data is often not meaningful as the location of sensors and impact positions do not coincide. Reciprocity of the virtual point receptance however should be reciprocal, and can therefore be used to assess the transformation quality.

Let i and j denote two different DoFs from the set of virtual point DoFs. Then a non-dimensional frequency dependent reciprocity value between 0 and 1 is defined by:

$$\chi_{ij} = \frac{(H_{ij} + H_{ji})(H_{ji}{}^* + H_{ji}{}^*)}{2(H_{ij}{}^* H_{ij} + H_{ji}{}^* H_{ji})} \tag{29}$$

This formula originates from the FRF input-output coherence function for the two measurements H_{ji} and H_{ij}. It shows the similarity in both amplitude and phase between the two virtual point FRFs.

4 SUMMARY

In this paper the theory behind the virtual point transformation is presented from a modal reduction perspective. We have shown that by weakening the interface problem, one only couples the rigid motion described by the IDMs, while the residual motion is left free. By assigning a certain weighting matrix, one can control this residual and with that the transformation. Ways to construct different IDMs from the sensor and impact positions are discussed.

Also some practical aspects were discussed that one may encounter when doing experimental substructuring. It appeared that sensor and impact positioning should be thought out carefully beforehand, but can still be evaluated afterwards on the basis of a number of non-dimensional performance indicators.

REFERENCES

[1] Randall J. Allemang. The modal assurance criterion twenty years of use and abuse. *Sound and Vibration*, pages 14–21, August 2003.

[2] R.R.J. Craig and M.C.C. Bampton. Coupling of substructures using Component Mode Synthesis. *AIAA Journal*, 6:1313–1319, 1968.

[3] D. de Klerk. *Dynamic Response Characterization of Complex Systems through Operational Identification and Dynamic Substructuring*. Phd thesis, Delft University of Technology, http://www.3me.tudelft.nl/live/pagina.jsp?id=73932050-a4ca-46b5-bd9b-d98b8a52dbe6, 2009.

[4] D. de Klerk, D.J. Rixen, and J. de Jong. The Frequency Based Substructuring Method reformulated according to the Dual Domain Decomposition Method. In *Proceedings of the XXIV International Modal Analysis Conference*. Society for Experimental Mechanics, 2006.

[5] D. de Klerk, D.J. Rixen, and S.N. Voormeeren. A General Framework for Dynamic Substructuring. History, review and classifcation of techniques. *AIAA Journal*, 46(8), 2008.

[6] D. de Klerk, D.J. Rixen, S.N. Voormeeren, and F. Pasteuning. Solving the RDoF problem in Experimental Dynamic Substructuring. In *Proceedings of the XXVI International Modal Analysis Conference, Orlando, FL*, Bethel, CT, 2008. Society for Experimental Mechanics.

[7] D. de Klerk and S.N. Voormeeren. Uncertainty Propagation in Experimental Dynamic Substructuring. In *Proceedings of the XXVI International Modal Analysis Conference, Orlando, FL*, Bethel, CT, 2008. Society for Experimental Mechanics.

[8] M.L.M Duarte and D.J. Ewins. Some Insights into the Importance of Rotational Degrees of Freedom and Residual Terms in Coupled Structure Analysis. In *Proceedings of the XIII International Modal Analysis Conference, Nashvill, TN*, pages 164–170, Bethel, CT, 1995. Society for Experimental Mechanics.

[9] T.S. Edwards. Implementation of Admittance Test Techniques for High-precision Measurement of Frequency Response Functions. In *Proceedings of the XXXI International Modal Analysis Conference*. Society for Experimental Mechanics, 2013.

[10] J. Harvie and P. Avitabile. Effects of precise FRF measurements for Frequency Based Substructuring. In *Proceedings of the XXXI International Modal Analysis Conference, Los Angeles, CA*, Bethel, CT, 2013. Society for Experimental Mechanics.

[11] B. Jetmundsen, R.L. Bielawa, and W. G. Flannelly. Generalized frequency domain substructure synthesis. *Journal of the American Helicopter Society*, 33(1):55–64, 1988.

[12] W. Liu and D.J. Ewins. The Importance Assessment of RDOF in FRF Coupling Analysis. In *Proceedings of the XVII International Modal Analysis Conference, Orlando, FL*, pages 1481–1487, Bethel, CT, 1999. Society for Experimental Mechanics.

[13] J.C. O'Callahan, I.W. Lieu, and C.M. Chou. Determination of Rotational Degrees of Freedom for Moment Transfers in Structural Modifications. In *Proceedings of the III International Modal Analysis Conference, Orlando, FL*, pages 465–470, Bethel, CT, January 1985. Society for Experimental Mechanics.

[14] F. Pasteuning. Experimental Dynamic Substructuring and its Application in Automotive Research. Master's thesis, TU Delft, Department of Engineering Mechanics, 2007.

[15] D.J. Rixen. How Measurement Inaccuracies Induce Spurious Peaks in Frequency Based Substructuring. In *Proceedings of the XXVI International Modal Analysis Conference, Orlando, FL*, Bethel, CT, 2008. Society for Experimental Mechanics.

[16] M.V. van der Seijs, D. de Klerk, D.J. Rixen, and S. Rahimi. Validation of current state Frequency Based Substructuring Technology for the characterisation of Steering Gear – Vehicle Interaction. In *Proceedings of the XXXI International Modal Analysis Conference, Los Angeles, CA*, Bethel, CT, 2013. Society for Experimental Mechanics.

[17] S.N. Voormeeren. Improvement of Coupling Procedures and Quantification of Uncertainty in Experimental Dynamic Substructuring Analysis; Application and Validation in Automotive Research. Master's thesis, TU Delft, 2007.